Residual semi-crystalline particles released during enzymatic degradation of plastics

Michael Schindler and Ludwik Leibler
Gulliver, École Supérieure de Physique et Chimie Industrielles, Paris Sciences et Lettres Université, CNRS, Paris 75005, France[*]
(Dated: Monday, 10th August 2026 at 16:12)

Enzymatic recycling of plastics is limited by the presence of semi-crystalline spherulites that are recalcitrant to enzymatic depolymerization. Depending on the quality of the waste stream and its treatment history, a large volume fraction of the material actually remains in form of connected clusters of such spherulites. We build on a recently published numeric method to predict the number, the connectivity, and the morphology of these clusters as an outcome of enzymatic degradation. When applied to PET waste, our method predicts that the resulting aggregates are loosely connected, "fluffy" structures with a high surface-to-volume ratio, accompanied by smaller clusters following a continuous size distribution. By providing a quantitative framework for understanding the microparticle production during the depolymerization, these findings should assist choosing a suitable downstream treatment, such as filtering or flocculation. This work could thus help to advance the enzymatic depolymerization technologies.

I. INTRODUCTION

The enzymatic degradation of polymer waste has emerged as a promising route for chemical recycling, offering true circularity in the usage of plastic resources and mild reaction conditions compared to other chemical methods [1–3]. Enzymatic degradation allows breaking down polymer chains into short pieces and finally into monomers, which can then be reused to make fresh virgin plastics, without the quality loss that is observed in other techniques. Semi-crystalline polymers, however present a challenge to this method: while amorphous regions are readily broken down by enzymes, ordered crystalline domains do not offer sufficient chain mobility and degradable site accessibility, and are thus depolymerized less efficiently [2, 4–14] and about an order of magnitude more slowly. Indeed, crystalline domains are not perfect monocrystals, often they are spherulites that grew from a nucleation center. They have lamellar structure, alternating crystalline and disordered amorphous layers [12]. Such confined and constrained amorphous domains within the spherulites are less accessible to enzymes and more recalcitrant to enzyme-catalyzed depolymerization than amorphous matrix. Amorphous regions within spherulites are thus depolymerized more slowly than fully amorphous polymers [8, 11]. In semi-crystalline polymer waste, the degradation kinetics is therefore coupled to polymer morphology [8, 15, 16]. Amorphization pretreatments alleviate this problem, but amorphization is never complete. Moreover, to be efficient depolymerization has to be carried out above the glass transition temperature, at which further crystallization can occur. This concerns in particular all semi-crystalline polyesters, among which also poly(ethylene terephthalate) (PET). Understanding the crystalline morphology and its evolution during enzymatic treatment is therefore critical for predicting yields and timescales of the enzymatic degradation process.

* michael.schindler@espci.fr

Recent experimental and modelling work [17] has revealed that under typical conditions the enzymatic depolymerization of amorphous matrix competes with the growth of embedded spherulitic, partly crystalline, domains. The presence of both, the amorphous matrix and the spherulites, results from the pre-treatment of the plastic waste, in particular melting, rapid cooling, and mechanical grinding. This competition between depolymerization and spherulite growth then determines the final yield and the timescale of the degradation process. The undegraded, residual material represents a significant fraction of the initial polymer mass. Depending on the quality of the waste stream and its treatment history, at least 40% of the material actually remains in form of spherulitic clusters [17, figure 12].

Questions naturally turn to how to further process the leftover material. Beyond its total volume, also the morphology of the residual material plays an important role: Rather than yielding a uniform reduction in particle size, the process generates a heterogeneous population of clusters of crystalline spherulites that are eventually released into the surrounding solution. Moreover, a closer look on these spherulites reveals that they are not totally crystalline but consist of lamellae or similarly ordered stacks, with amorphous material between them [17–19]. For example in reference [17, Figure 10], efficient amorphization pretreatment yielded an initial crystallinity degree as low as 10%, which corresponds to a spherulite volume of already 35%. The small-scale amorphous phase within the spherulites can be depolymerized, but it is less accessible to enzymes than the bulk amorphous matrix and has less mobility, and it is thus depolymerized on a larger timescale [7]. It is thus useful to differentiate between a "first stage", in which the bulk amorphous matrix is depolymerized, and in which partly crystalline spherulites grow; and a "second stage", in which also the amorphous material within the spherulites is depolymerized [17, figure 12]. The two stages are not strictly successive in time, they refer to the different timescales involved.

The rate at which the slow "second-stage" depolymer-

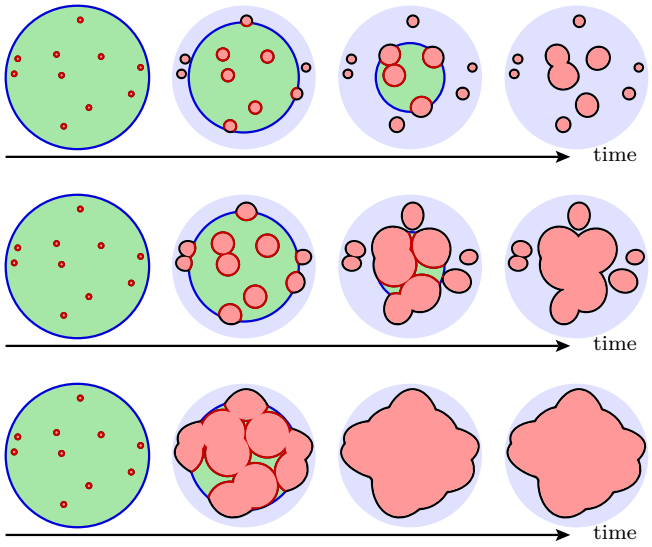

Figure 1. Possible outcomes of the enzymatic degradation of a plastic particle, for different processing conditions: many small spherulites (top row), or various sizes of spherulite clusters (middle row), or a single compact cluster of spherulites (bottom row). The amorphous matrix (green) is degraded, the spherulites (red) grow (and possibly nucleate) within the amorphous matrix, finally remaining as connected clusters of egg-shaped objects (black curves).

ization happens, strongly depends on the morphology of the clusters that result from the faster "first stage": If the clusters expose much surface to the enzymes, for example if they are rather fractal objects with thin local structures, they are depolymerized at a higher rate than if they were a dense compact object, exposing little surface. Knowing the morphology of this material is thus interesting and important. In the present paper we analyze the morphology of the clusters resulting from the "first stage".

The morphology of the undegraded polymers might influence the overall design of the recycling process. There are various decisions to take. Either the crystalline spherulites are kept in the enzyme solution until they are also degraded on a long or very long timescale (the *waiting strategy*); or they have to be flocculated or filtered out and treated similarly as the initial plastic waste, that is melted, cooled, milled, and depolymerized (the *filtering strategy*). In order to take such a design decision, it is important to know the size distribution of the spherulites produced (for the filtering strategy) and how much surface they potentially expose to enzymes (for the waiting strategy). For example, many very small spherulites in the outcome propose themselves for the waiting strategy, whereas compact big particles require to be filtered and subjected to another round of the whole process.

Despite their importance for process optimization, the geometric and statistical properties of these residual clusters have received limited attention [8, 20, 21]. Key questions remain: How does the density and growth rate of spherulites determine cluster morphology? Under what conditions do spherulites remain isolated versus forming large aggregates? What surface area do these clusters expose for further enzymatic attack? Answering these questions requires connecting the microscopic parameters of spherulite nucleation and growth to the macroscopic observables of cluster size distributions and surface properties.

Here we address these questions using a geometric model that treats degradation as the coupled evolution of a shrinking amorphous sphere containing randomly distributed, growing spherulites. Building on our previous work [17], which focused on the total amount of degraded and remaining volumes, we now characterize the residual clusters themselves. By solving the model equations numerically and tracking the connectivity of overlapping spherulites, we identify when clusters detach from the degrading particle and determine their volume, surface area, and internal structure. Applying these numerics to the parameters we obtained in reference [17] for the experimental degradation of PET from different waste sources, allows us to make a prediction for the total amount and for the distribution of structure and size of the leftover crystalline clusters. Since experiments suggest that the depolymerization of spherulites is much slower than that of the amorphous matrix [17, figure 12], we neglect it in the model. This work thus answers the question how far depolymerization can go if only the amorphous matrix is degraded. It does not explicitly describe the depolymerization of inter-lamellar amorphous material in clusters. Instead, it provides the morphology of these clusters, which is useful for estimating their further degradation.

Our results demonstrate how the operating parameters of enzymatic degradation – temperature (which controls spherulite growth rate), residence time, and initial particle size – map onto a percolation phase diagram that predicts residual cluster morphology. This connection between process conditions and residual waste structure provides a much simpler but still quantitative framework for optimizing multi-stage degradation protocols: conditions which maintain subcritical spherulite density yield residues in small clusters only, amenable to rather quick secondary treatment, whereas supercritical conditions produce compact aggregates requiring repeated processing strategies such as mechanical separation and re-melting.

Our results further demonstrate how to predict cases in which remains a big structured cluster of spherulites. We develop a reduced model to predict the time of its formation, which marks also the end of the degradation process.

More broadly viewed, this work illustrates how concepts from soft matter physics – percolation transitions, surface-to-volume scaling, extreme value statistics, and the statistical mechanics of random geometric structures – illuminate practical problems in sustainable materials processing. The geometric model we employ is sufficiently simple to yield analytical insights while capturing the essential physics of competing degradation and crystallization. Extensions to more complex scenarios, includ-

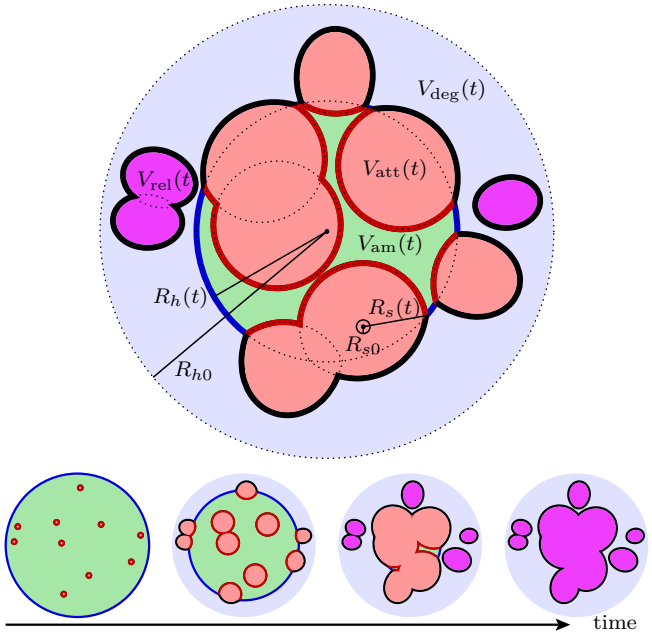

Figure 2. Top: the four different geometric volumes used in the model, at a given time t: Already degraded volume $V_{\rm deg}(t)$ (light blue), the amorphous matrix $V_{\rm am}(t)$ (light green), the volume of spherulite clusters still attached to the matrix $V_{\rm att}(t)$ (light red), and the volume of spherulite clusters not attached anymore $V_{\rm rel}(t)$ (light purple). The thick curves show the interfaces between these volumes, and the dotted curves indicate spherical shapes. Bottom: the same volumes at consecutive times.

ing nucleation, polydisperse spherulite populations, non-uniform distributions, and anisotropic growth, represent natural next steps in developing predictive models for polymer degradation.

The paper is organized as follows: Section II reviews the geometric model and establishes notation. Section III presents numerical solutions of the model, including the time-resolved release of spherulite clusters into the solute. It provides the distributions of cluster sizes and their surface properties. In sections IV and V we develop two sub-models which predict the two relevant timescales of the process, one for the formation of a dominant cluster, the other for its "release" into the solute. Section VI applies the theory to parameters obtained from experimental data.

II. SUMMARY OF THE GEOMETRICAL MODEL

In reference [17] we presented a geometrical model for the enzymatic degradation of plastic waste, where the waste is thermally pre-treated and shred into small particles. The main issue addressed by the model is that these polymer particles are semi-crystalline: They contain partly crystalline spherulites which are degraded much more slowly. The nucleation and growth of spherulites inside the otherwise amorphous plastic particles is a result of the chosen degradation conditions. In particular, the reaction temperature must be high enough such that the polymer chains in the amorphous parts are sufficiently mobile for the enzymes to cleave them. At this temperature crystalline spherulites nucleate and grow in time. The overall degradation is then a competition between depolymerization of the amorphous matrix at its surface and the growth of embedded spherulites.

We take spherical geometry for both the degrading particle and for the growing spherulites. The degradation of the amorphous matrix is modelled by the shrinking of a sphere, having at time t the radius

$$R_h(t) = R_{h0} + \dot{R}_h t, \quad \text{with constant } \dot{R}_h < 0. \tag{1}$$

The radius decreasing linearly in time reflects that the volume change of amorphous matrix material is proportional to the area of surface it exposes to enzymes.

Each spherulite has a given initial radius and grows at constant growth rate where it is in contact with the amorphous matrix. For the sake of simplicity we take the same initial radius and the same growth rate for all spherulites, and we take the spherulites' radius of curvature to grow linearly in time,

$$R_s(t) = R_{s0} + \dot{R}_s t, \quad \text{with constant } \dot{R}_s > 0. \tag{2}$$

Initially, the spherulite positions are uniformly randomly distributed within the amorphous sphere, such that they do not stick out. Their number is denoted by N_s and their density of centers (number per volume) by N_s'.

As the radii evolve in time, the embedded spherulites can come into contact with each other, and the amorphous matrix is degraded from the outside, such that spherulites can start to stick out. Spherulites are modelled to be non-degradable by enzymes, such that the part of the spherulites outside the amorphous matrix does not change anymore. The combined dynamics finally leaves clusters of spherulites as a remainder. The shapes at some intermediate times are shown in figures 1 and 2. The characteristic egg-like shape of a spherulite, with its long axis oriented towards the center of the particle, is the result of intersecting a growing with a shrinking sphere. Figure 2 depicts volumes of three different phases: The amorphous matrix $V_{\rm am}(t)$ in light green; the volume $V_{\rm deg}(t)$ of matrix having been degraded up to time t in light blue; and the spherulite volume $V_{\rm sph}(t)$ which has some (partly) crystalline structure. These three volumes always add up to the initial volume $V_{\rm tot} := 4\pi R_{h0}^3/3$, which will serve to normalize them,

$$V_{\rm am}(t) + V_{\rm sph}(t) + V_{\rm deg}(t) = V_{\rm tot}. \tag{3}$$

Within the volume $V_{\rm sph}(t)$ of the spherulite/crystalline phase, we differentiate between those spherulite clusters having been released into the surrounding and those clusters still attached to the amorphous matrix – either embedded in it, or partly sticking out. The former have

volume $V_{\mathrm{rel}}(t)$ and are drawn in light purple in figure 2, whereas the latter have volume $V_{\mathrm{att}}(t)$ and are drawn in light red. They satisfy

$$V_{\mathrm{sph}}(t) = V_{\mathrm{att}}(t) + V_{\mathrm{rel}}(t). \tag{4}$$

Figure 2 further shows the interfaces between the different volumes. The rate at which amorphous volume is converted into spherulite volume is proportional to the area of the amorphous–spherulite interface (dark red in figure 2). This quantity is – up to a constant scaling factor corresponding to the internal degree of crystallinity of the spherulites – accessible by experimental techniques [15, 17, 22, 23].

At the same time as spherulites are shaped by the receding amorphous matrix, they block access of enzymes to this matrix and thus effectively reduce the degradation rate. The degradation of the amorphous volume is thus proportional to the area of the exposed amorphous–solute interface (thick dark blue curves in figure 2). The characteristic timescale of degradation is given by

$$\tau_h := R_{h0} \,/\, |\dot{R}_h|, \tag{5}$$

which is the time a purely amorphous particle takes to degrade. We denote units of length and time by $\mathcal{L}$ and $\mathcal{T}$, respectively.

Finally degraded volume

Solutions to equations (1)–(3) have been presented in reference [17] in form of the time evolution of the volumes involved. Figure 3 shows such solutions for three prototypical choices of parameters. The main quantities of interest in reference [17] were the final yield, i.e. the amount of degraded material, and the timescale on which it is obtained. We discussed the influence of the parameters R_{h0}, R_{s0}, $\dot{R}_h$, $\dot{R}_s$, and N'_s.

Remaining spherulite clusters

Since we model the spherulites to be inert to enzymes, and the spherulites grow only inside the amorphous sphere, where they are in contact with the amorphous matrix. Thus, spherulite clusters, consisting of partly overlapping spherulites, grow while at least one of their member spherulites is still attached to the matrix. Once the last member spherulite has detached from the matrix, the cluster of spherulites is considered as "released" and diffusing away from the particle.

III. RELEASED CLUSTERS OF SPHERULITES

The numerical solution of the model equations, applied to explicit sets of spherulite positions, gives access to much more detailed information than we presented in

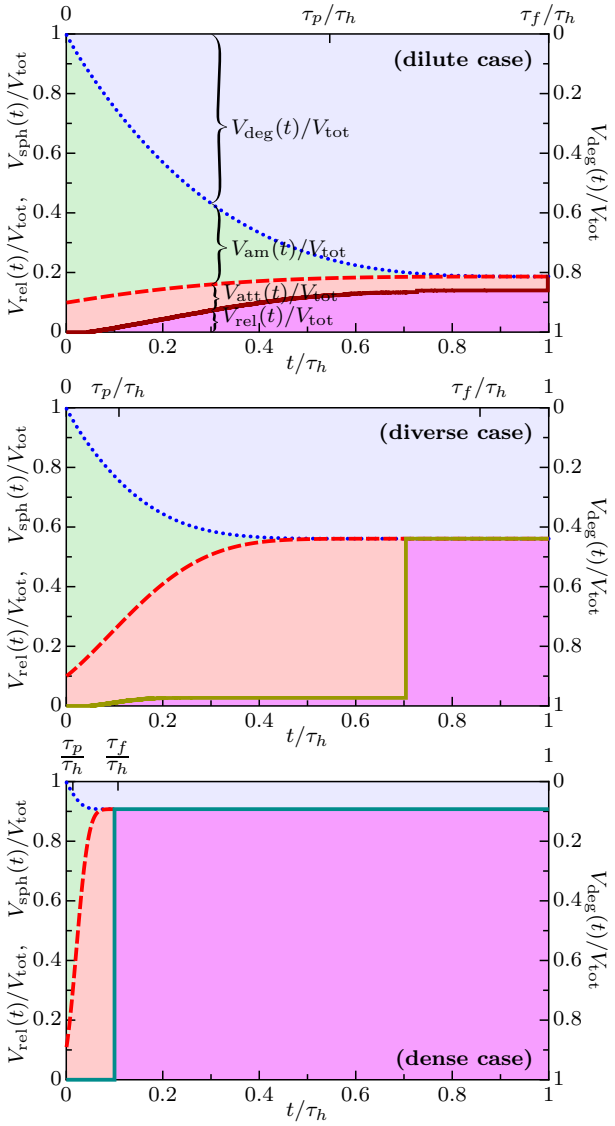

parameters:	R_{s0}	$\dot{R}_s$	N'_s	R_{h0}	$\dot{R}_h$
dilute case	$0.02\mathcal{L}$	$0.02\mathcal{L}/\mathcal{T}$	$2387/\mathcal{L}^3$	$\mathcal{L}$	$-\mathcal{L}/\mathcal{T}$
diverse case	$0.02\mathcal{L}$	$0.10\mathcal{L}/\mathcal{T}$	$2387/\mathcal{L}^3$	$\mathcal{L}$	$-\mathcal{L}/\mathcal{T}$
dense case	$0.02\mathcal{L}$	$0.80\mathcal{L}/\mathcal{T}$	$2387/\mathcal{L}^3$	$\mathcal{L}$	$-\mathcal{L}/\mathcal{T}$

Figure 3. Evolution in time of the four volumes $V_{\mathrm{rel}}(t)$, $V_{\mathrm{att}}(t)$, $V_{\mathrm{am}}(t)$, $V_{\mathrm{deg}}(t)$. As guides to the eye, we use the same color code for these volumes as in figure 2. The dashed red curves and the solid stepwise lines refer to the left axes, the blue dotted curves refer to the right axes. The characteristic percolation time (τ_p) and the characteristic final time of filling (τ_f) – see below, in equations (7) and (13) – are marked on the upper time axis of each graph. Top graph: spherulites remain individual or form small clusters (dilute case). Middle graph: diverse sizes of smaller clusters are released, with one bigger clusters at late time. Bottom graph: the growing spherulites remain attached to the amorphous phase only for short time and are released as one big cluster (dense case). The table gives the model parameters used for the graphs.

reference [17]. There we provided the amount of degraded volume and the total amount of spherulite volume. The numerical method uses adapted Delaunay/Voronoi tessellations to integrate volume and surface of *all individual spherulites*, and also to determine which of them overlap. We thus have access to their connectivity and can identify all connected clusters of spherulites [24]. For each such cluster we determine whether it is still attached to the amorphous matrix, that is whether one of its spherulites overlaps with the shrinking sphere. Once a cluster has detached, it is considered "released", and we have access to its volume and to its surface, by adding up the contributions from all spherulites taking part in the connected cluster.

The numerical technique thus allows to model the creation of spherulite clusters during the degradation process. Figure 3 shows the evolution in time of the four different volumes in the model: The blue dotted curves, referring to the right axes, show the volume $V_{\mathrm{deg}}(t)$ having been degraded up to time t. The red dashed curves, referring to the left axes, show the volume of spherulites, $V_{\mathrm{sph}}(t)$. Thus, the volume of amorphous matrix, $V_{\mathrm{am}}(t)$ is the vertical distance between blue and red curve – see the vertical braces in the top panel of the figure. The spherulite volume $V_{\mathrm{sph}}(t)$ is split into two parts, namely $V_{\mathrm{rel}}(t)$, the volume of spherulite clusters having detached from the amorphous matrix and been released into the solute, and $V_{\mathrm{att}}(t)$ the volume of spherulites still connected to the amorphous matrix at time t, either directly or indirectly as part of a cluster still being attached. The identification of the four volumes in figure 3 has been eased by using a background coloring scheme using the same colors as in figure 3.

In figure 3 the two types of spherulite volumes, the released clusters and the attached ones, are separated by lines consisting of many discrete steps. At each step a spherulite cluster is released from the particle. There are many small steps, hardly visible individually, and a final (big) step which is the "release" of the remaining spherulite cluster, when all amorphous matrix has been degraded.

In the top panel of figure 3 the overall degradation is very good, and only 19% of the initial material is finally found in form of spherulites. The spherulites are continuously released as very small clusters until the end of the process. This case corresponds to small and slowly growing spherulites. In the middle panel spherulites grow faster, leading to the release of a few very small clusters in the beginning; the main volume, however, is connected to a main cluster until the end of the depolymerization at quite late time. The final cluster has around 50% of the initial volume. In the bottom panel the spherulites grow so fast that they clump together quickly and form one dense cluster after short time. There are no small clusters, and only a few percent of the matrix material could be degraded.

Figure 4 shows volume and surface of every released cluster, including the final cluster, for the three cases given in figure 3. The "dilute" case is dominated by individual

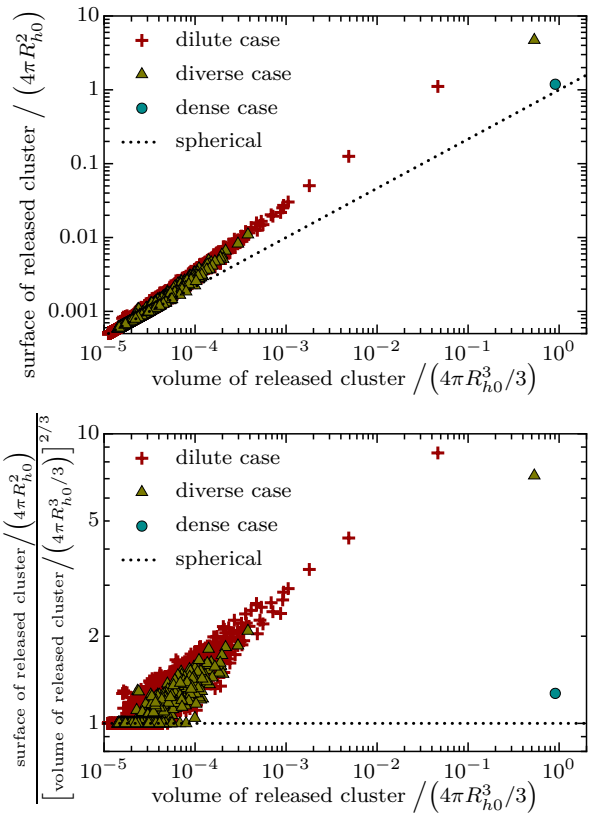

Figure 4. Top graph: Volume and surface of every cluster formed in the evolutions shown in figure 3. Bottom graph: The same data, plotted on a different vertical axis which shows how "sphere-like" the cluster is. Numeric values are given in table I.

	dilute	diverse	dense
N_s	9939	9939	9939
number of clusters	3700	738	1
$\sum_c \frac{\text{volume of cluster } c}{4\pi R_{h0}^3/3}$	0.19	0.56	0.91
$\sum_c \frac{\text{surface of cluster } c}{4\pi R_{h0}^2}$	5.9	5.6	1.2
$\frac{\sum_c \frac{\text{surface of cluster } c}{4\pi R_{h0}^2}}{\left[\sum_c \frac{\text{volume of cluster } c}{4\pi R_{h0}^3/3}\right]^{2/3}}$	18.2	8.2	1.27
$\max_c \frac{\frac{\text{surface of cluster } c}{4\pi R_{h0}^2}}{\left[\frac{\text{volume of cluster } c}{4\pi R_{h0}^3/3}\right]^{2/3}}$	8.6	7.2	1.27
$\max_c \frac{\text{volume of cluster } c}{4\pi R_{h0}^3/3}$	0.047	0.53	0.91
maximal number of spherulites in a cluster	1533	8648	9939

Table I. Quantitative measures of the spherulite clusters shown in figure 4.

sphere-like spherulites; there are also many small clusters of spherulites partly overlapping. In the opposite, "dense" case only one cluster remains. Its shape is close to a sphere, having only little extra surface, which comes from spherulites bulging out a bit. In the intermediate case of "diverse" cluster sizes, we find again small ones, but there is also a dominating cluster, which is loosely connected and has a large surface. It contains about half of the initial volume. Table I provides quantitative information about the clusters, in particular their number, the sum of their volumes and of their surface areas. Also, the largest clusters are quantified there.

In order to obtain a clearer idea of how much more surface these clusters expose, in figure 4 we plot the same data in two different ways. In the lower panel, the vertical axis provides a surface-to-volume ratio for each cluster, which compares the cluster's surface with the surface of a sphere having the same volume as the cluster. This measure gives an idea how much excess surface the cluster has due to its complex structure. We find that in the "dense" case volume and surface are close to those of a sphere, its surface is only 1.27 times larger, see again table I. It is thus a compact, round object; the lowest row in figure 1 gives a good idea of how the "dense" final cluster might look like.

Very differently, in the "diverse" case we find much more surface, with a total surface-to-volume ratio of 8.2. Already the dominating cluster has a ratio of 7.2.

Finally, in the "dilute" case we find only small clusters, the largest cluster volume has only 4.7% of the total cluster volume. The many small clusters together have huge excess surface, with a surface-to-volume ratio of 18.2. This is not surprising, since we have 3700 clusters, formed from the initial 9939 spherulites, thus on average only three spherulites per cluster. Nevertheless, there are also bigger clusters, up to 1533 spherulites for the largest one. This cluster has a similar structure as the dominating one in the "diverse" case, its surface-to-volume ratio is 8.6.

The dramatic increase of surface, relative to volume, of small or loosely connected clusters is a true advantage for a possible second stage of degradation. With eight or eighteen times more surface even a five times slower degradation can be useful.

Figure 4 gives an indication how compact a cluster is, based on its volume and surface. It gives a rough idea of the cluster's size – but rather indirectly. In figure 5 we show a histogram of the sizes of these clusters. For complex objects made of several spherulites, the term "size" is not as well-defined as are volume and surface. Here, we measured the extent of the cluster parallel to each Cartesian coordinate axis, that is the smallest and the largest Cartesian coordinate of all its spherulites. The "size" referred to in figure 5 is the largest such extent.

In figure 5 we see the same qualitative picture as in figure 4: The "dilute" case results in a continuum of clusters, where larger clusters are increasingly rare. The "various" case exhibits a discontinuous distribution of sizes, with small clusters and a large one, essentially of the same size as the initial particle. The gap between the sizes is well visible. The "dense" case results only in large clusters, again of the same size as the initial particle.

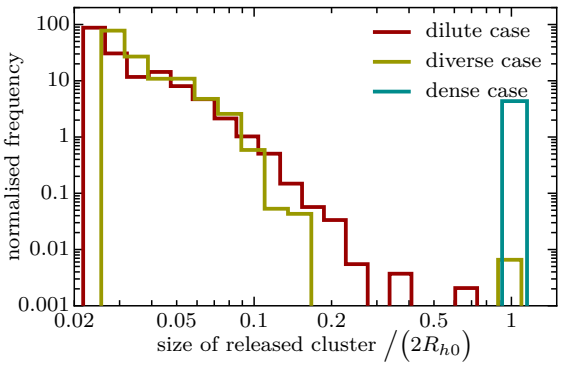

Figure 5. Histogram of sizes of the clusters formed in the evolutions shown in figure 3. Here, "size" refers to the maximal extent along the three Cartesian coordinate axes.

IV. FOCUS MODEL: PREDICTING THE PERCOLATION TIME

In figures 3, 4 and 5 we find a crossover between two extremes, one being mainly isolated spherulites, or very small clusters of them, the other being a single big cluster of nearly all spherulites. We can rationalize this result using a simplification that is known in the scientific literature of percolation thresholds as the "continuum percolation model"[1] [25–28]. There, many spheres are randomly placed in infinite or periodic space. Mutual overlap of spheres defines a "connectivity" between them, such that "clusters" of connected spheres can be identified. The main question addressed in the context of percolation is whether there is a dominant cluster.

Let us simplify the setting of our model and neglect the time evolution of spherulites and of particles. We do numerical calculations of the percolation test, adapted to our setting of spherulites within a particle: In three spatial dimensions we randomly place N_s small spheres of radius R_s in a big sphere of radius $R_h > R_s$. Their spatial distribution is chosen such that the centers are uniformly distributed inside the large sphere. We then determine the connectivity of the small spheres and count for each connected cluster the number of involved small spheres. We further count how many clusters we have for a given number of involved spheres. The whole process is repeated M times to obtain better statistics, and it is repeated for various values of R_s. Figure 6 presents the result: For every observed number of spheres in a cluster

[1] Various names have been given to the model, such as "off-lattice percolation", "fully penetrable spheres", "overlapping spheres", the "Swiss-cheese model", or the "Poisson blob model."

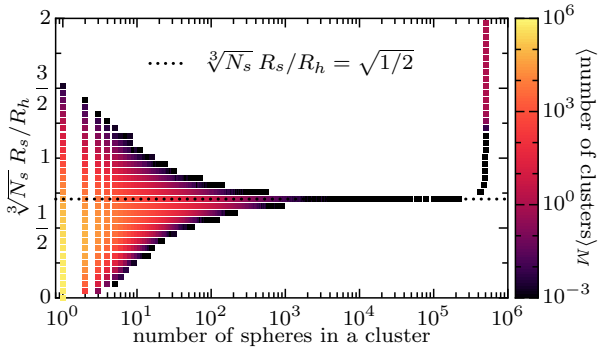

Figure 6. The percolation problem: Numerically determined frequencies of cluster sizes, when many (N_s=5×10^5, fixed) small spheres (radius R_s, varying) are placed uniformly randomly inside one big sphere (radius R_h=1, fixed). The numbers of clusters are averaged over many (M=10^3, fixed) repetitions of the random placing. Dots are drawn where at least one cluster comprising the given number of spheres has been observed. Their color indicates how many such clusters have been observed, averaged over the repetitions. The dotted line is an estimate for the percolation threshold.

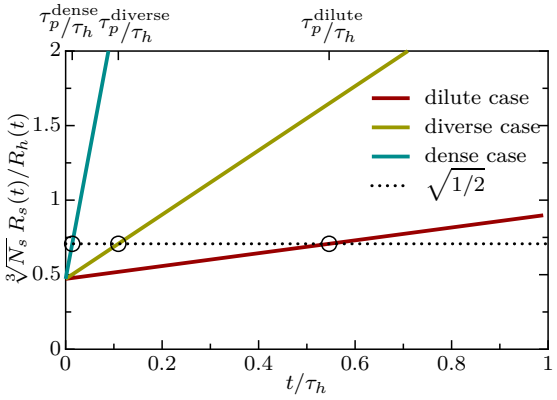

Figure 7. The percolation indicator $\sqrt[3]{N_s}R_s(t)/R_h(t)$ as a function of time, for the same parameters as for the curves in figure 3. The times when they cross the percolation threshold (dotted line) are marked by circles and on the upper time axis.

the figure shows a little square. Its color encodes how often this cluster size has been observed, averaged over the repetitions.

The percolation transition is very well visible in figure 6: There is a threshold value near $\sqrt[3]{N_s}R_s/R_h \approx \sqrt{1/2}$, see also reference [29]. Below the threshold, for small or few spherulites, cluster sizes behave monotonously, small clusters are very numerous, bigger clusters less numerous, and there is no dominating cluster. Above the threshold, one cluster dominates, combining nearly all spheres, accompanied by only a few additional small clusters.

The percolation model allows to understand the difference between the three cases in figures 3, 4 and 5 qualitatively and quantitatively. In figure 7 we draw the parameters as a function of time, such that we can trace their combination relevant for the clustering, namely $\sqrt[3]{N_s}R_s/R_h$ over time. These parameter functions are linear, essentially showing the growth of the spherulite radius $R_s(t)$. The times when the parameter lines cross the percolation threshold are marked with circles in figure 7. They are given by resolving the percolation condition

$$\sqrt[3]{N_s}R_s/R_h = \sqrt{1/2} \tag{6}$$

for the time, yielding the characteristic time of percolation

$$\tau_p := \frac{1}{\dot{R}_s}\left(\frac{\sqrt{1/2}}{\sqrt[3]{N'_s 4\pi/3}} - R_{s0}\right). \tag{7}$$

Inserting the parameters of figure 3, we obtain

	τ_p/τ_h
dilute case	0.55
diverse case	0.11
dense case	0.014.

(8)

These values are also indicated on the upper time axes of the graphs in figure 3. In the top two graphs we see that τ_p indicates the typical timescale when small spheres add up to a considerable volume. This is precisely the setting of the percolation approximation.

With the percolation model in mind, it becomes an evident fact that for an initial volume of spherulites higher than 0.35%, more precisely for $V_{\rm sph}(0)/V_{\rm tot} > 2^{-3/2}$, the dilute case is impossible. There will always be a dominant cluster, either densely packed or fluffy.

V. FOCUS MODEL: PREDICTING THE TIME WHEN DEPOLYMERIZATION ENDS

In the previous section we presented a reduced effective model for the percolation time τ_p. Here we proceed to develop another reduced effective model focusing on the "release" time of a dominant remaining cluster, τ_f. This time marks the end of the depolymerization of the particle and is well visible as a pronounced final step in each graph of figure 3. In the detailed numerics of figure 3, the time of "release" is defined to be the moment when the shrinking sphere, which represents the amorphous matrix, exposes no surface to the enzymes anymore. Some enclosed cavities of amorphous matrix may still be left, but they are small and will disappear shortly after. Effectively, the time of release nearly coincides with the time when the sphere representing the amorphous matrix is completely filled by spherulites. We are thus looking for the formation time of a dense core of the remaining cluster.

Our reduced model should therefore answer the question at what (growing) radius $R_s(\tau_f)$ spherulites, which have been placed randomly in space at a given density (of centers) N'_s, fill space completely.

We consider again a Delaunay tessellation, in which every vertex carries one spherulite center. A Delaunay cell is then a tetrahedron (simplex) having four such Delaunay

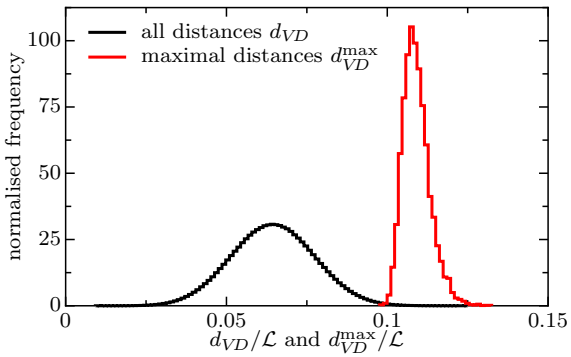

Figure 8. Black line: Histogram of the distances d_{VD} from every Voronoi vertex to the corners of its dual Delaunay cell, taken from 10^3 tessellations of uniformly random points in a periodic cube of side-length $\mathcal{L}$. Red line: Histogram of the largest distance $d_{VD}^{\max}$ in each of 10^4 tessellations. In both cases the density of input Delaunay vertices is $N_s' = 2387/\mathcal{L}^3$. Both histograms are normalized to have unit integral.

vertices at its corners, and it corresponds to one Voronoi vertex of the dual tessellation. The dual (Voronoi) vertex has the same distance d_{VD} to all four vertices of the Delaunay cell. This means that the growing spherulites, centered in the corners of the Delaunay tetrahedron, will meet in that very dual Voronoi point at the moment they completely fill the Delaunay tetrahedron. At that time all four spherulite radii will be equal to the distance d_{VD} of this cell. Since the positions of spherulites are random variables, also the distance d_{VD} and the complete-filling time are random variables, for each Delaunay cell.

The latest closure of any point in the whole tessellation will take place at the Voronoi vertex which has the largest distance to its Delaunay neighbors. This is the respective maximum of all d_{VD} in this tessellation, $d_{VD}^{\max}$, which is also a random variable. We will ask for its distribution and its mean value. The question for the maximum of several random variables is a classical one, treated in the statistics community under the term *extreme value statistics* [30–33].

The task can be solved numerically: We generate a set of uniformly random input vertices, calculate the Delaunay tessellation and its dual. We then measure the distance between Voronoi vertex and Delaunay vertices in each Delaunay cell, and determine the largest such distance in the tessellation. In order to obtain good statistics, we repeat the process for many tessellations which differ by their random positions of input vertices, keeping the number of Delaunay input points the same. Finite-size effects are limited to a minimum by performing the tessellations in a periodic cube of side-length $\mathcal{L}$.

Figure 8 shows the resulting histograms of both types of distances. The black line is the histogram of all Delaunay-to-Voronoi distances d_{VD}, collected from all distances in many tessellations. Its shape is close to the probability density function of a normal distribution, but its lower tail is of course limited by $d_{VD} > 0$, and its upper tail

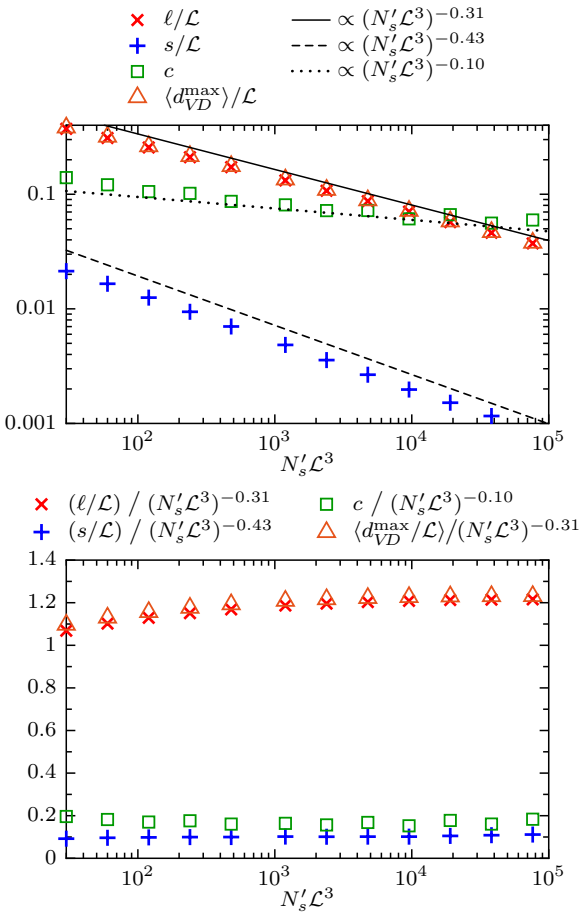

Figure 9. Dependence on the input density N_s' of the three parameters ℓ, s, c of the generalized extreme-value distribution, together with its mean value $\langle d_{VD}^{\max}\rangle$. The scaling exponents are fitted by the eye.

by the periodic box. The red line in figure 8 is the histogram of the respective largest such distance found in each tessellation, $d_{VD}^{\max}$, collected from many tessellations. This histogram is close to a *generalized extreme-value distribution* [33] which is parameterized by a shape parameter $c > 0$, a location parameter ℓ, and a scaling parameter s, and which has the probability density function [34]

$$\rho(d; c, \ell, s) = \frac{1}{s} \exp\Big(-\Big[1 - \frac{d-\ell}{s/c}\Big]^{\frac{1}{c}}\Big) \Big[1 - \frac{d-\ell}{s/c}\Big]^{\frac{1}{c}-1}. \quad (9)$$

The mean is given in terms of the gamma function [35, 36],

$$\langle d\rangle = \ell + \frac{s}{c}\big(1 - |\Gamma(c+1)|\big). \quad (10)$$

It remains to determine the dependence of parameters c, ℓ, s on the density N_s' of input points (spherulite centers). We varied N_s' and fitted the function (9) to the observed distances $d_{VD}^{\max}$. The best-fit parameters are given in figure 9. In the upper graph we observe that the parameters follow power laws, and we determine their exponents. In the lower graph we determine the prefactors.

The mean of the maximal distance then scales as

$$\langle d_{VD}^{\max}\rangle \approx 1.2\mathcal{L}\,(N_s'\mathcal{L}^3)^{-0.31}, \tag{11}$$

with better matches for large N_s'. With expression (11) we obtain the average time τ_f when the last little cavity of amorphous matrix is being converted into spherulite material,

$$\tau_f = \min\Big\{\frac{1}{\dot R_s}\Big(\langle d_{VD}^{\max}\rangle - R_{s0}\Big), \tau_h\Big\} \tag{12}$$

$$\approx \min\Big\{\frac{1}{\dot R_s}\Big(1.2\mathcal{L}\,(N_s'\mathcal{L}^3)^{-0.31} - R_{s0}\Big), \tau_h\Big\}. \tag{13}$$

As argued at the beginning of the present section, this is close to the moment we called *release of the final (big) cluster* in the previous sections, and which implies the end of the depolymerization process, and which is marked by the last big step in figure 3. Inserting the parameters of figure 3, we obtain the values

	τ_f/τ_h
dilute case	1.00
diverse case	0.86
dense case	0.11.

(14)

These values are also marked on the upper time axes of figure 3. In the "dilute" case the formula (13) hits the maximal allowed value, τ_h, which is the correct behavior also observed in figure 3. In the "diverse" case, the formula slightly overestimates the release time – either because the latter is stochastic in nature and figure 3 shows just one realization, or because the difference between the first closure of the amorphous matrix' exposed surface and the last filling of its bulk by spherulites is not as small as we expected. In the "dense" case, the formula correctly predicts the release time of the cluster.

VI. EXAMPLE: PREDICTIONS FOR PET WASTE DEPOLYMERIZATION

In reference [17] we fitted the model parameters to experimental data. There, two different sources of PET were treated, from bottle flakes, and from textile waste [23], and they were degraded at different temperatures. Fitting the model to the experimental data yielded the parameters given in the table of figure 10. In particular, the initial sizes of the particle and of the spherulites are taken to be

$$\begin{aligned} R_{h0} &= 80\mu\text{m}, \\ R_{s0} &= 1.5\mu\text{m} \quad \text{or} \quad 1.6\mu\text{m}. \end{aligned} \tag{15}$$

The solution of the model equations for these parameters are reproduced in the graphs of figure 10. The style of the graphs is the same as of those in figure 3, showing the four volumes $V_{\rm deg}(t)$, $V_{\rm am}(t)$, $V_{\rm att}(t)$, $V_{\rm rel}(t)$. For a detailed interpretation of these curves see reference [17].

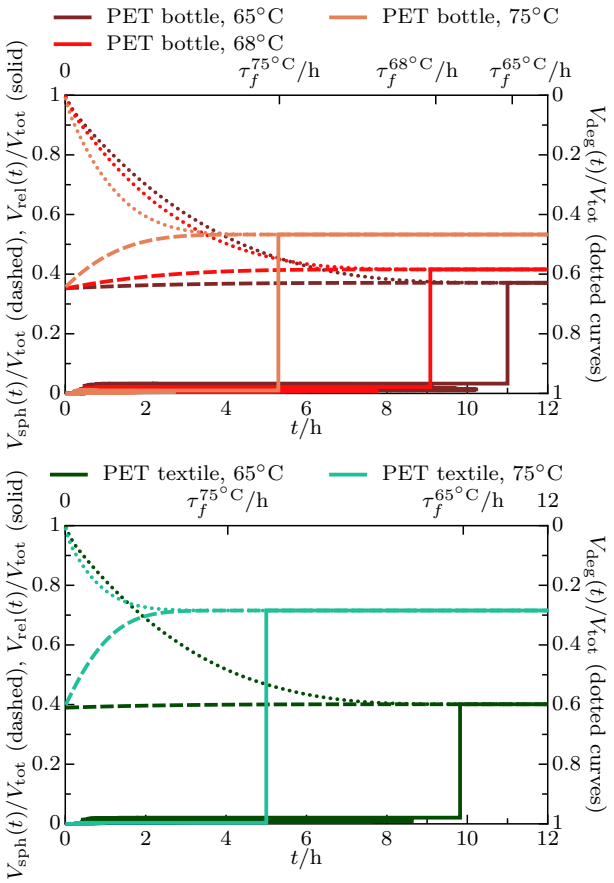

parameters:	R_{s0}	$\dot R_s$	N_s'	R_{h0}	$\dot R_h$
bottle 65°C	1.5μm	0.01μm/h	0.03/(μm)^3	80μm	−7.20μm/h
bottle 68°C	1.5μm	0.05μm/h	0.03/(μm)^3	80μm	−8.68μm/h
bottle 75°C	1.5μm	0.23μm/h	0.03/(μm)^3	80μm	−15.02μm/h
textile 65°C	1.6μm	0.01μm/h	0.03/(μm)^3	80μm	−8.08μm/h
textile 75°C	1.6μm	0.49μm/h	0.03/(μm)^3	80μm	−13.71μm/h

Figure 10. Release of the spherulite clusters (continuous lines), and evolution in time of the four volumes $V_{\rm rel}(t)$, $V_{\rm att}(t)$, $V_{\rm am}(t)$, $V_{\rm deg}(t)$. The plot style is the same as in figure 3: $V_{\rm deg}(t)$ (dotted curves) refer to the right axis; $V_{\rm sph}(t)$ (dashed curves) and $V_{\rm rel}(t)$ (solid lines) refer to the left axis. The colors refer to different materials. The model parameters used for the graphs, as given in the table, are obtained from experimental data from two different waste sources at different temperatures, see reference [17].

We can now add the numerical prediction for the remaining spherulite clusters to the expected outcome of these experiments. The release curves of spherulite clusters, obtained from detailed numerics, are shown in the graphs of figure 10 as continuous lines. The formation of spherulite clusters has two characteristic times, as discussed in sections IV and V, namely τ_p for the occurrence of a globally connected dominant cluster, and τ_f of the final release of the remaining cluster. We obtain their

overall quantities:	bottle 65°C	bottle 68°C	bottle 75°C	textile 65°C	textile 75°C
N_s	63811	63694	64038	63681	64138
number of clusters	2429	1539	771	1474	267
$\left(\sum_c \text{volume of cluster } c\right) \Big/ \left(4\pi R_{h0}^3/3\right)$	0.37	0.42	0.53	0.40	0.72
$\left(\sum_c \text{surface of cluster } c\right) \Big/ \left(4\pi R_{h0}^2\right)$	15.2	15.4	14.8	15.4	10.7
$\frac{\sum_c \text{surface of cluster } c}{4\pi R_{h0}^2} \Big/ \left[\sum_c \frac{\text{volume of cluster } c}{4\pi R_{h0}^3/3}\right]^{2/3}$	29.5	27.7	22.5	28.4	13.4
quantities of the dominant cluster c:					
number of spherulites in cluster c	58642	60506	62622	60790	63732
$\left(\text{volume of cluster } c\right) \Big/ \left(4\pi R_{h0}^3/3\right)$	0.34	0.39	0.52	0.38	0.71
$\left(\text{surface of cluster } c\right) \Big/ \left(4\pi R_{h0}^2\right)$	13.6	14.4	14.3	14.5	10.5
$\frac{\text{surface of cluster } c}{4\pi R_{h0}^2} \Big/ \left[\sum_c \frac{\text{volume of cluster } c}{4\pi R_{h0}^3/3}\right]^{2/3}$	28.1	26.8	22.1	27.6	13.2

Table II. Quantitative measures of the spherulite clusters shown in figure 11.

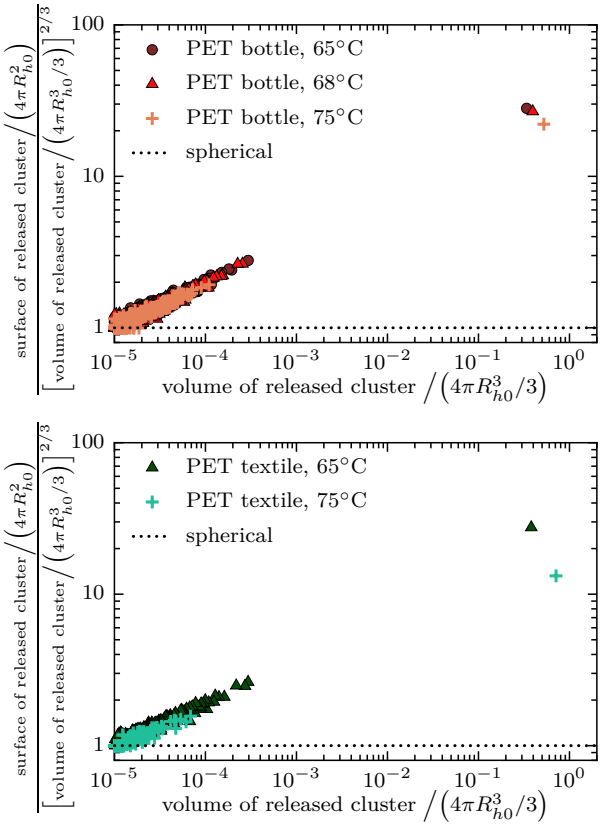

Figure 11. Geometric measures of every spherulite cluster released in the evolutions shown in figure 10. Numeric values are given in table II.

values from equations (7) and (13),

	τ_h	τ_p	τ_f	τ_f/τ_h
bottle 65°C	11.1h	−9.3h	11.1h	1
bottle 68°C	9.2h	−2.2h	9.2h	1
bottle 75°C	5.3h	−0.5h	5.3h	1
textile 65°C	9.9h	−22.2h	9.9h	1
textile 75°C	5.8h	−0.4h	4.0h	0.7 .

(16)

The values for the percolation time τ_p are all negative, which means that the initial parameters are already above the percolation threshold. It is therefore impossible to find here the "dilute case" that we saw in figures 3, 4, and 5. The experimental conditions used on the given materials always lead to a dominant remaining cluster of spherulites, either to a densely packed one or to a fluffy one. There are also additional small clusters.

The characteristic times in equation (16) are marked also on the upper time axes in the graphs of figure 10. They coincide very well with the release times of the final particle, which are obtained from the detailed numerical solution of the model, and which is visible as the big steps in the curves indicating the cluster releases (thick continuous lines). This coincidence is not a surprise, as equation (16) gives nearly all release times as the largest possible ones, τ_h, with one exception, $\tau_f^{75°C}$. We thus learn that the experimental conditions were such that the final clusters were released at the end of the degradation process, with the degradable matrix remaining accessible to enzymes down to the center of the particle. The resulting clusters of spherulites must have a fluffy structure with deep holes down to the center.

Figure 11 corroborates this conclusion. It shows the surface and volume of all spherulite clusters obtained. In all five cases we see a clear separation of clusters into one dominant and into very small clusters. The dominant cluster is always made of around 90% of the spherulites, and it always has a high or very high surface-to-volume

ratio, which is characteristic for a fluffy, loosely connected structure. The numeric values of these ratios are given in the bottom row of table II.

We remind the reader that the numbers presented in table II and in the figures result from numerical modeling. We rely on the model parameters we have fitted to experimental data in reference [17]. What does our prediction in table II imply in terms of particles per liter? In reference [23] we used around 5mg/mL of polyester powder, up to size 150μm, in 1mL of buffer solution. Thus, there were around 1.7×10^3 particles in 1mL solution, initially. According to table II, for example for PET bottles processed at 65°C, these particles are reduced to 34% of their initial volume, and around 4.1×10^6 additional small particles are split off from them. These millions of small particles represent only 3% of the initial volume.

VII. CONCLUSION

For enzymatic depolymerization, plastic material is thermally pre-treated and mechanically broken into amorphous particles. The process is then a competition between depolymerization at the surface and growth of recalcitrant embedded spherulites. Under typical conditions, the undegraded, residual material represents a significant fraction of the initial polymer mass. Depending on the quality of the waste stream and its treatment history, at least 40% of the material actually remains in form of spherulitic clusters.

Here, we characterize the morphology of these spherulitic clusters. We extended the numerics of our geometric model for enzymatic degradation of plastic particles from reference [17], such that it yields also the clusters of connected crystalline spherulites. The numerics make extensive use of Delaunay/Voronoi tessellations.

In the degradation dynamics of plastic particles we identify three prototypical cases which differ in the quantity and in the properties of the resulting spherulite clusters. They are presented in figures 3, 4 and 5: If the spherulites are few and grow slowly, they form only small clusters. At intermediate growth rate, called the "diverse case", they form both small clusters and a dominant one. The latter cluster is a loosely connected, fluffy structure of many spherulites. It has holes and crevasses nearly down to its center. It is further characterized by a very large surface-to-volume ratio. If the spherulites' growth rate is high, they all form a single, filled cluster with a low surface-to-volume ratio close to that of a sphere. We provide quantitative measures of these clusters, both their overall quantities, and also those of the largest/dominant cluster.

We find that the formation of spherulite clusters is characterized by two timescales, one for the formation of a dominant cluster, the other for the formation of a dense core in such a cluster. We provide analytic estimates for both timescales – for each of them we focus the model to a simpler, effective one that allows for an alternative treatment. One of them is similar to a percolation model, well-studied in the statistical physics of disordered media, the other one makes use of Delaunay/Voronoi tessellations and extreme-value statistics.

We apply the model to parameters fitted to and matching the outcome of experiments on the degradation of PET from two different sources of waste, treated at different temperatures. The degradation dynamics and the resulting spherulites are presented in figures 10 and 11. We find that under the given experimental conditions the degradation was always in the "diverse case", leading to a dominant remaining cluster of spherulites. The "dilute case" is excluded by means of the high initial crystallinity. The "dense case" would also be possible, but the growth rates of spherulites turn out to be small enough for this case not to occur.

The model predicts the resulting semi-crystalline particles as fluffy assemblies of small spherulites, which have practically no solid core and a very high surface-to-volume ratio. Their size is nearly the size of the initial particle, which results from the grinding pre-treatment; in the example examined in this paper the initial particle size was around 160μm. In addition to the dominant cluster, the depolymerization produces very small spherulite clusters. In our case of PET these small microparticles have sizes between 3μm and 30μm. Together they make up only a few percent of the initial volume, see table II. However, the number of these small clusters is huge: In our example of PET depolymerization, they are three orders of magnitude more numerous than the initial particles (between 267 and 2429, see table II). The exact numbers depend on the material, they are influenced by the pre-treatment, and they depend on the nucleation rate and growth rate of spherulites under depolymerization reaction conditions.

The presented model is intended to draw attention to the microparticle production during the depolymerization process and to help to find efficient strategies to deal with this leftover material in the overall design of the recycling process.

[1] F. Kawai, T. Kawabata, and M. Oda, Current knowledge on enzymatic PET degradation and its possible application to waste stream management and other fields, Applied Microbiology & Biotechnology **103**, 4253 (2019).

[2] T. B. Thomsen, C. J. Hunt, and A. S. Meyer, Influence of substrate crystallinity and glass transition temperature on enzymatic degradation of polyethylene terephthalate (PET), New Biotechnology **69**, 28 (2022).

[3] M. C. Shehbas, D. S. Desai, T. M. Mathew, and K. M. Nampoothiri, Microbial enzymes for plastic degradation: A comprehensive review of current status and emerging trends, Biodegradation **37**, 30 (2026).

[4] R. Wei, G. von Haugwitz, L. Pfaff, J. Mican, C. P. S. Badenhorst, W. Liu, G. Weber, H. P. Austin, D. Bednar, J. Damborsky, and U. T. Bornscheuer, Mechanism-based design of efficient PET hydrolases, ACS Catalysis **12**, 3382 (2022).

[5] F. Kawai, R. Iizuka, and T. Kawabata, Engineered polyethylene terephthalate hydrolases: Perspectives and limits, Applied Microbiology and Biotechnology **108**, 404 (2024).

[6] A. Patel, A. C. Chang, U. Abid, C. Ayafor, H.-W. Wong, D. Xie, and M. J. Sobkowicz, Effects of copolymer structure on enzyme-catalyzed polyester recycling, Journal of Polymers and the Environment **32**, 3961 (2024).

[7] K. Welzel, *Einfluss der chemischen Struktur auf die enzymatische Hydrolyse von Polyester-Nanopartikeln*, Ph.D. thesis, Gemeinsame Naturwissenschaftliche Fakultät der Technischen Universität Carola–Wilhemina zu Braunschweig, Braunschweig (2003).

[8] T. Gaillard, M. George, E. Gastaldi, F. Nallet, and P. Fabre, An experimental and theoretical study of the erosion of semi-crystalline polymers and the subsequent generation of microparticles, Soft Matter **15**, 8302 (2019).

[9] A. Patel, A. C. Chang, A. Mastromonaco, M. A. Diaz, S. Perry, O. Ferki, C. Ayafor, U. Abid, H.-W. Wong, D. Xie, and M. J. Sobkowicz, Aqueous buffer solution-induced crystallization competes with enzymatic depolymerization of pre-treated post-consumer poly (ethylene terephthalate) waste, Polymer **285**, 126370 (2023).

[10] A. C. Chang, A. Patel, S. Perry, Y. V. Soong, C. Ayafor, H.-W. Wong, D. Xie, and M. J. Sobkowicz, Understanding consequences and tradeoffs of melt processing as a pretreatment for enzymatic depolymerization of poly(ethylene terephthalate), Macromolecular Rapid Communications **43**, 2100929 (2022).

[11] T. B. Thomsen, K. Almdal, and A. S. Meyer, Significance of poly(ethylene terephthalate) (PET) substrate crystallinity on enzymatic degradation, New Biotechnology **78**, 162 (2023).

[12] S. W. Schubert, T. B. Thomsen, K. S. Clausen, A. Malmendal, C. J. Hunt, K. Borch, K. Jensen, J. Brask, A. S. Meyer, and P. Westh, Relationship of crystallinity and reaction rates for enzymatic degradation of poly(ethylene terephtalate), PET, ChemSusChem **17**, e202301752 (2024).

[13] S. Kaabel, J. P. D. Therien, C. E. Deschênes, D. Duncana, T. Friščić, and K. Auclair, Enzymatic depolymerization of highly crystalline polyethylene terephthalate enabled in moist-solid reaction mixtures, Proceedings of the National Academy of Sciences **118**, e2026452118 (2021).

[14] A. Zaker and K. Auclair, Impact of ball milling on the microstructure of polyethylene terephthalate, ChemSusChem **18**, e202401506 (2025).

[15] M. Ye, X. Wang, W. Huang, J. Hu, and H. Bu, Fast crystallization of poly(ethylene terephthalate), Journal of Thermal Analysis **46**, 905 (1996).

[16] R. Wei, D. Breite, C. Song, D. Gräsing, T. Ploss, P. Hille, R. Schwerdtfeger, J. Matysik, A. Schulze, and W. Zimmermann, Biocatalytic degradation efficiency of postconsumer polyethylene terephthalate packaging determined by their polymer microstructures, Advanced Science **6**, 1900491 (2019).

[17] M. Schindler, H. Garate, and L. Leibler, Theory for enzymatic degradation of semi-crystalline polymer particles, Macromolecules **59**, 3226 (2026).

[18] M. L. Di Lorenzo, Crystallization of poly(ethylene terephthalate): A review, Polymers **16**, 1 (2024).

[19] B. Wunderlich, Reversible crystallization and the rigid amorphous phase in semicrystalline macromolecules, Progress in Polymer Science **28**, 383 (2003).

[20] X. Han and J. Pan, A model for simultaneous crystallisation and biodegradation of biodegradable polymers, Biomaterials **30**, 423 (2008).

[21] X.-F. Wei, A. J. Capezza, Y. Cui, L. Li, A. Hakonen, B. Liu, and M. S. Hedenqvist, Millions of microplastics released from a biodegradable polymer during biodegradation/enzymatic hydrolysis, Water Research **211**, 118068 (2022).

[22] D. Wang, F. Luo, Z. Shen, X. Wuab, and Y. Qi, A study on the crystallization behavior and mechanical properties of poly(ethylene terephthalate) induced by chemical degradation nucleation, RSC Advances **7**, 37139 (2017).

[23] H. Garate, C. Freymond, L. Breloy, M. Schindler, J. Pallis, B. Gibbs, B. Mansaku, Y. Rondelez, C. Creton, A. D. Griffiths, and L. Leibler, Reactive mixing enables enzymatic depolymerization of recalcitrant or unsortable polyester wastes, Proceedings of the National Academy of Sciences **122**, e2505611122 (2025).

[24] The CGAL Project, CGAL 5.6.2 - profiling tools, hash map, union-find, modifiers (CGAL Editorial Board, 2024) `https://doc.cgal.org/5.6.2/Miscellany/classCGAL_1_1Union__find.html` accessed Jan 2025.

[25] J. Quintanilla and S. Torquato, Clustering properties of d-dimensional overlapping spheres, Physical Review E **54**, 5331 (1996).

[26] K. W. Kratky, The area of intersection of n equal circular disks, Journal of Physics A: Mathematical and General **11**, 1017 (1978).

[27] D. Stauffer and A. Aharony, *Introduction to Percolation Theory*, revised 2nd ed. (Taylor & Francis, 1994).

[28] R. Meester and R. Roy, *Continuum percolation* (Cambridge University Press, 1996).

[29] S. Torquato, Effect of dimensionality on the continuum percolation of overlapping hyperspheres and hypercubes, The Journal of Chemical Physics **136**, 054106 (2012).

[30] L. de Haan and A. Ferreira, *Extreme Value Theory: An Introduction* (Springer, 2006).

[31] S. I. Resnick, *Extreme Values, Regular Variation and Point Processes* (Springer, 1987).

[32] S. Coles, *An Introduction to Statistical Modeling of Extreme Values* (Springer, 2001).

[33] *Tutorial: Generalized Extreme Value Distribution*, The SciPy community, 1.17.0 ed. (26 Feb 2026), `https://docs.scipy.org/doc/scipy/tutorial/stats/continuous_genextreme.html`.

[34] *Reference manual for scipy.stats.genextreme*, The SciPy community, 1.17.0 ed. (26 Feb 2026), `https://docs.scipy.org/doc/scipy/reference/generated/scipy.stats.genextreme.html#scipy.stats.genextreme`.

[35] *Manual for scipy.special.gamma*, The SciPy community, 1.17.0 ed. (26 Feb 2026), `https://docs.scipy.org/doc/scipy/reference/generated/scipy.special.gamma.html#scipy.special.gamma`.

[36] *Source code for the mean of scipy.stats.genextreme*, The SciPy community, 1.17.0 ed. (26 Feb 2026), `https://github.com/scipy/scipy/blob/v1.17.0/scipy/stats/_continuous_distns.py#L3449-L3454`.